Journal of Alloys and Compounds 498 (2010) 179–184

Contents lists available at ScienceDirect

Journal of Alloys and Compounds

journal homepage: www.elsevier.com/locate/jallcom

Synthesis, characterization, and activities of visible light-driven Bi_2O_3–TiO_2 composite photocatalysts

Yuande Liu[a], Feng Xin[a,*], Fumin Wang[a], Shanxia Luo[a], Xiaohong Yin[b]

[a] School of Chemical Engineering and Technology, Tianjin University, Tianjin 300072, China
[b] School of Chemistry and Chemical Engineering, Tianjin University of Technology, Tianjin 300384, China

ARTICLE INFO

Article history:
Received 8 December 2009
Received in revised form 17 March 2010
Accepted 17 March 2010
Available online 23 March 2010

Keywords:
Bi_2O_3
TiO_2
Composite photocatalysts
Photocatalytic degradation

ABSTRACT

A series of Bi_2O_3–TiO_2 composite photocatalysts were prepared with a facile nonaqueous sol–gel method through varying the Bi–Ti atomic ratio and calcination temperature. The catalyst structures had been extensively characterized by using X-ray photoelectron spectroscopy (XPS), high-resolution transmission electron microscopy (HRTEM), X-ray diffraction (XRD), UV–visible diffuse reflectance spectroscopy (UV–vis DRS). The characterization results revealed that all of the Bi_2O_3–TiO_2 composites exhibited smaller crystallite size, higher thermal stability and stronger absorbance in visible light range than pure TiO_2. The photocatalytic activities of as-prepared catalysts were evaluated by the degradation of methyl orange (MO). The results showed that the Bi–Ti atomic ratio of 0.0175 was an optimum in the photocatalytic activities under visible light irradiation and the calcination temperature affected both the physicochemical properties and photocatalytic activities of the catalysts.

XPS and XRD were further used to characterize the stability of the photocatalyst, which maintained a high activity without obvious deactivation after five recycles of the degradation.

1. Introduction

Environmental pollution is a major concern worldwide. Especially, the organic dye pollutants in liquid waste have become the serious problem in the wastewater treatment [1]. As we all know, the high costs associated with the technologies of water purification (e.g. biodegradation, physical entrainment and incineration) forced great efforts to develop not only effective but also cheaper innovative processes for environment cleaning [2,3]. Besides well-established techniques, semiconductor photocatalysis has played a key role in degradation of organic pollutants in waste water, especially those from the textile and the photographic industries. Among various oxide semiconductor photocatalysts, TiO_2 has been proved to be one of the most effective and suitable photocatalyst for environmental applications because of its biological and chemical inertness, stability against photocorrosion, non-toxicity, high redox ability and lower cost [4,5]. But its relatively wide band gap (3.2 eV for anatase) and the relatively high rate of photogenerated electron–hole recombination limit its further application in the visible light region (400 nm < λ <700 nm), which accounts for 43% of the incoming solar energy [6].

To overcome the above two drawbacks, one of the most promising ideas is coupling TiO_2 with other narrow band gap semiconductors with matching band potentials [7–17], which can construct a heterojunction structure. In a coupled semiconductor system, the narrow band gap semiconductor can be excited by visible light irradiation and some of the photogenerated electrons or holes will then be transferred to TiO_2 vis heterojunction interface, leading to efficient charge separation. The extensively studied TiO_2-based doped photocatalysts include Bi_2WO_4–TiO_2 [11], WO_3–TiO_2 [12], ZnO–TiO_2 [13], $FeTiO_3$–TiO_2 [14], SiO_2–TiO_2 [15], Bi_2O_3–TiO_2 [16,17] and so on.

Bi_2O_3 is a significant metal-oxide semiconductor with a direct band gap 2.8 eV, which can be excited by visible light, but the photocatalytic activity of Bi_2O_3 is low due to the photocorrosion and fast recombination of photogenerated electron–hole pairs [18]. In recent years, the development of Bi_2O_3–TiO_2 composite photocatalyst that can work effectively under visible light irradiation with photochemical stability is a very hot topic in photocatalysis research. Cao and his coworkers used evaporation-induced self-assembly (EISA) method and P123 surfactant as a template to synthesize Bi_2O_3–TiO_2 with ordered mesoporous structure [16]. Jing's group prepared Bi_2O_3 surface-modified TiO_2 nanoparticle by sol-hydrothermal process of $Ti(OBu)_4$, followed by post-treatment with an appropriate amount of bismuth nitrate solution [17]. Xu et al. synthesized Bi_2O_3–TiO_2 composite film by refluxing acidic solution (pH 2) of isopropyl alcohol, $Ti(OBu)_4$ and α-Bi_2O_3 [19]. In this paper, we prepared Bi_2O_3–TiO_2 composite photocatalysts

* Corresponding author. Tel.: +86 22 27409533; fax: +86 22 27892359.
E-mail address: xinf@tju.edu.cn (F. Xin).

0925-8388/$ – see front matter © 2010 Elsevier B.V. All rights reserved.
doi:10.1016/j.jallcom.2010.03.151

with a nonaqueous sol–gel method by using cetyl trimethylammonium bromide (CTAB) as a dispersant, which could improve the dispersibility of particles during ultrasonication and promote stable dispersions of solids in different media [20–22]. The photodegradation of MO was employed to evaluate the photocatalytic activities of the Bi_2O_3–TiO_2 catalysts, with a 500W Xe lamp equipped with an UV-cut-off filter ($\lambda > 400$ nm) as the light source. The activities on different atomic ratios of Bi–Ti and calcination temperatures were tested and discussed. Moreover, the stability of the Bi_2O_3–TiO_2 photocatalysts after multiple photocatalytic degradation runs was also evaluated.

2. Experimental

2.1. Preparation of Bi_2O_3–TiO_2

All chemicals were analytical grade without further purification and purchased from Tianjin jizhun chemical company. In a typical synthesis procedure, 0.1 g CTAB was dissolved in 15 mL absolute ethanol under vigorous stirring at room temperature. Then the resulting solution was ultrasonicated for 15 min before mixing with 6 mL butyl titanate. After 20 min ultrasonication, a homogeneous solution was formed and subsequently heated to 82 °C. At this time, a certain amount of bismuth(III) nitrate pentahydrate was added into the solution with vigorous stirring, and a yellowish sol was obtained after 30 min ultrasonication and 180 min stirring. The resulting colloid was aged at room temperature for 24 h and 85 °C for 10 h, and then calcined in air for 8 h at 420, 520 and 620 °C (2 °C/min), respectively. Finally, a series of samples with Bi amount ranging from 0.0000 to 0.0234 were prepared and named as Bi–Ti–*x*–*y*, where *x* denotes the Bi–Ti atomic ratio and *y* defines the calcination temperature (°C). The pure TiO_2 sample was also prepared by the same procedure except adding the bismuth(III) nitrate pentahydrate.

In our process, it was necessary to add CTAB as the surface dispersant to make bismuth(III) nitrate pentahydrate evenly and stably suspend in ethanol and form uniform suspensions.

2.2. Characterization

The determination of crystallite sizes and identification of the pure TiO_2, Bi_2O_3–TiO_2 were carried out by XPS, HRTEM, XRD, and UV–vis DRS. XPS was recorded on a PHI-5600 multitechnique system with a monochromatic Al Kα source (Physical Electronics) operated at 150W (15 kV, 10 mA). TEM and HRTEM images were obtained on a Tecnai G2 F20 S-TWIN instrument operated at 200 kV accelerating voltage. The XRD was performed on a Bruke/D8-Advance with Cu Ka radiation ($k = 0.1518$ nm) at a scan rate of $0.02^\circ\ S^{-1}$. The operation voltage and current were maintained at 40 kV and 100 mA. UV–vis DRS was recorded by Shimadzu UV-2550 spectrophotometer by using $BaSO_4$ as a reference in wavelength of 200–800 nm.

2.3. Evaluation of photocatalytic activities

Methyl orange (MO) was chosen as the target pollutant for photocatalytic activities, since it is a typical azo dye and difficult to degrade. In the optical system used for the photocatalytic reaction, a 500W Xe lamp from Beijing Institute of Electric Light Source was located at 16 cm over the surface of reaction solution, and in light way a 400 nm cut-off filter was used to remove all the UV lights with wavelength shorter than 400 nm. In each experiment, 0.08 g of photocatalyst was added into 80 mL of MO solution with a concentration of 10 mg/L in a reactor with a cooling jacket. All catalysts were sieved to obtain particles of 0.12–0.15 mm size. Before irradiation, the suspension was isolated light and stirred for 50 min to establish sorption equilibrium. The concentration of MO at this point was taken as the initial value for calculation. In certain time interval, 3 mL solution was sampled from the suspension and immediately centrifuged, and the concentration of MO was measured by UV–vis spectrophotometer at 464 nm wavelength.

The stability of the catalysts was tested by repeating the same experiment. Once each run of photodegradation experiment finished, the used catalyst was centrifuged, washed with ethanol and dried before reuse.

3. Results and discussion

3.1. XPS analysis

High-resolution XPS was used to elucidate the detailed surface chemical compositions and their electronic states of the samples. As shown in Fig. 1a, there were two strong peaks at 158.7 and 163.9 eV in the high-resolution spectra were assigned to $Bi_{4f7/2}$ and $Bi_{4f5/2}$, respectively. It was in agreement with the reported pure Bi_2O_3 values [23], showing the +3 valence state of Bi cation. In Fig. 1b, the

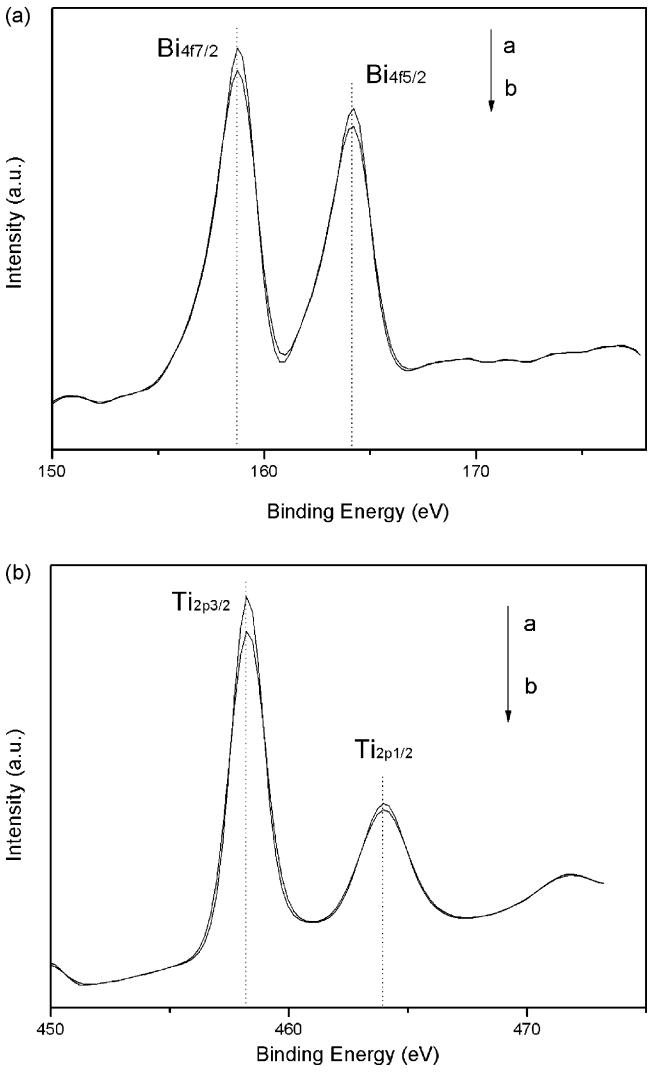

Fig. 1. (a) High-resolution scanning XPS spectra of Bi 4f (curve a) before photodegradation and (curve b) after photodegradation and (b) high-resolution scanning XPS spectra of Ti 2p (curve a) before photodegradation and (curve b) after photodegradation.

peaks of $Ti_{2p3/2}$ and $Ti_{2p1/2}$ were centered at 458.20 and 464.7 eV, which showed the main valence of Ti in the prepared catalysts is +4 and Ti^{4+} is in tetrahedral coordination with oxygen. These results suggested that the Bi_2O_3 and TiO_2 were present mainly as separate phases in Bi_2O_3–TiO_2 composites, respectively.

3.2. TEM and HRTEM analyses

In order to investigate the nanocrystalline nature of Bi_2O_3–TiO_2, the sample was characterized by TEM and HRTEM. The typical TEM of the Bi–Ti–0.0175–420 in Fig. 2a showed that the crystallite size was around 14 nm, which was in agreement with the latter obtained by XRD analysis, and the shape of particles was mainly spherical. HRTEM was used to further investigate the structural information of the Bi–Ti–0.0175–420 sample (Fig. 2b), which revealed that this sample was highly crystallized, as evidenced by well-defined lattice fringes. Many different lattice fringes could be found and allowed for identifying the crystallographic spacing of TiO_2 and Bi_2O_3. The fringes of $d = 0.352$ nm matched the (1 0 1) crystallographic plane of anatase TiO_2, while the fringes of $d = 0.325$ nm and $d = 0.271$ nm matched the (1 2 0) and (1 2 1) crystallographic planes of Bi_2O_3 nanoparticles, respectively. The

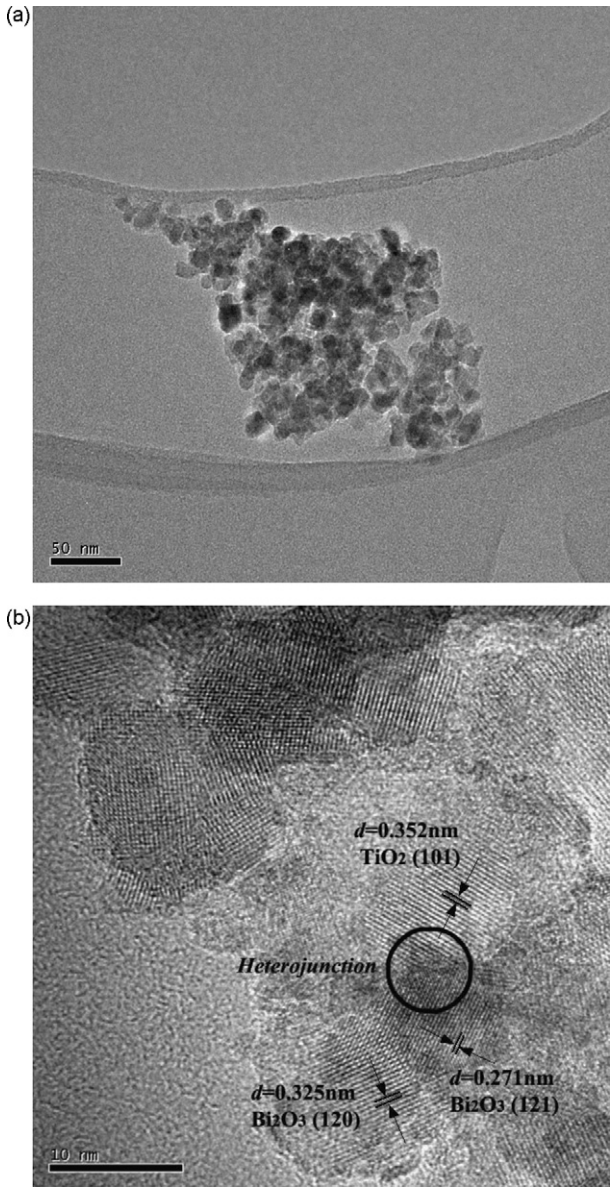

Fig. 2. (a) TEM images of Bi–Ti–0.0175–420 and (b) HRTEM images of Bi–Ti–0.0175–420.

HRTEM analysis further confirmed that Bi_2O_3 and TiO_2 coexisted in the resulting samples. Furthermore, an interconnected nanoparticular morphology was observed in Fig. 2b, which indicated a Bi_2O_3–TiO_2 nanocrystal heterojunction to be formed in the composite.

3.3. XRD analysis

XRD patterns in Fig. 3a showed that only anatase crystal phase presented in the Bi–Ti–*x*–420 samples, corresponding to the characteristic diffractive peaks around $2\theta = 25.25$, 37.88 and 48.00, respectively. Clearly, Bi did not replace Ti in TiO_2 frame because the radius of Bi^{3+} was 0.096 nm, which was larger than 0.068 nm of Ti^{4+}. No observation of Bi_2O_3 diffraction peaks was due to the low content of Bi_2O_3 and the extremely high dispersion of the Bi_2O_3 particles [16].

Based on the XRD results, the mean crystal sizes of Bi_2O_3–TiO_2 powders were calculated by the Scherrer equation. The particle sizes decreased with the increase of Bi–Ti proportion (Table 1),

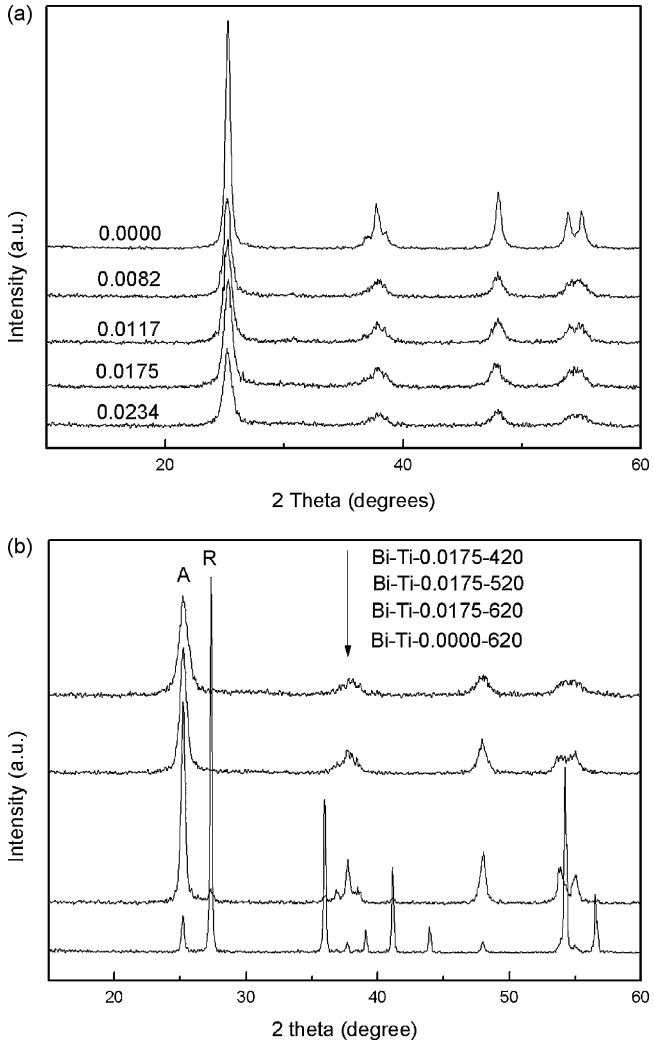

Fig. 3. (a) XRD patterns of the samples with different atomic ratios of Bi–Ti at 420 °C calcination and (b) XRD patterns of the Bi–Ti–0.0175 samples calcined at different temperatures.

which suggests the presence of Bi_2O_3 with high dispersion on TiO_2 particles could inhibit the crystal growth of TiO_2 during the calcination process. Furthermore, the XRD patterns of the Bi–Ti–0.0175 at different calcination temperatures in Fig. 3b demonstrated that Bi_2O_3 was capable of inhibiting the TiO_2 phase transformation from anatase-to-rutile in comparision with the Bi–Ti–0.0000–620 sample. Therefore, it could be concluded that the introduction of Bi_2O_3 could suppress the phase transformation and crystal growth of TiO_2, which maybe caused by hererojunction interface between Bi_2O_3 and TiO_2 nanocrystals in composite. In addition, the increase of calcination temperature resulted an increase of (1 0 1) diffraction peak intensity, indicating the crystal phase of TiO_2 became perfect, and some crystal grains agglutinated and became bigger.

3.4. UV–vis DRS and band gap

The optical properties of the Bi_2O_3–TiO_2 samples were measured by using UV–vis DRS. The results indicated that visible light was clearly absorbed by all the Bi–Ti–*x*–420 samples due to the contribution of Bi_2O_3 (Fig. 4a). The strong absorption of the Bi_2O_3–TiO_2 composites in the visible region implies efficient utilization of visible light for the photocatalytic reaction. Moreover, the plot of $(\alpha h\nu)^{1/2}$ versus the energy of light [24] afforded band gap energy

Table 1
Crystallite size (nm) of all the Bi–Ti–*x*–420 and Bi–Ti–*x*–520 samples.

Calcination temperature	Samples				
	Bi–Ti–0.0000	Bi–Ti–0.0082	Bi–Ti–0.0117	Bi–Ti–0.0175	Bi–Ti–0.0234
420 °C	19.50	16.47	15.88	13.97	12.68
520 °C	28.10	18.13	17.09	15.00	14.27

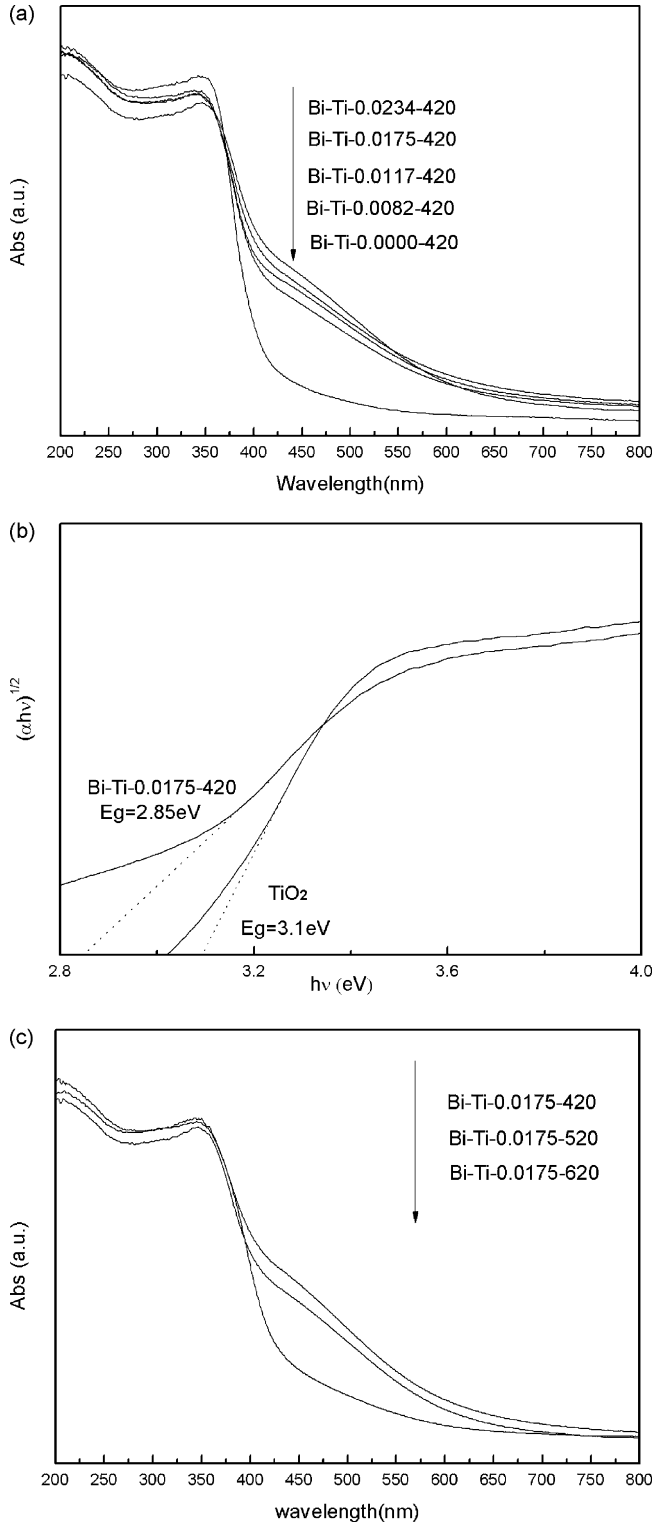

Fig. 4. (a) UV–vis spectra of Bi–Ti–*x*–420, (b) the optical absorption edges (eV) of Bi–Ti–0.0175–420 and (c) UV–vis spectra of the Bi–Ti–0.0175 samples at different calcination temperatures.

of 2.85 eV for Bi–Ti–0.0175–420 (Fig. 4b), which could be easily induced photoelectrons and holes by visible lights.

The UV–vis DRS of Bi–Ti–0.0175 samples calcined at different temperatures were shown in Fig. 4c. It can be seen that the Bi–Ti–0.0175 samples calcined at 420, 520 °C displayed similar absorbance for visible lights, suggesting that in the composite, Bi_2O_3 mainly resulted the spectral response in the visible region. However, with the increase of calcination temperature to 620 °C, the Bi–Ti–0.0175 sample showed a obviously weaker absorption in the visible light region than that of calcined at 420 and 520 °C, which might be due to the formation of a new phase of $Bi_4Ti_3O_{12}$ at 620 °C [25–27], but XRD was not sensitive enough to detect such minor phase to the samples.

3.5. Photocatalytic activity

The MO photolysis upon visible light irradiation in the blank experiment was not observable and under dark condition, no degradation of MO was detected for 8 h in presence of the photocatalysts. Therefore, both the illumination and the photocatalysts were essential for the highly efficient degradation. As shown in Fig. 5a, all of the Bi–Ti–*x*–420 catalysts significantly achieved faster MO photodegradation rates than pure TiO_2 self-made and commercial Degussa P25 TiO_2 under visible light irradiation. MO photodegradation was enhanced initially by increasing Bi–Ti proportion, and decreased thereafter while the Bi–Ti proportion reached a higher level. Clearly, there was an optimal Bi–Ti proportion of 0.0175 to exhibit the highest photocatalystic activity. When the Bi–Ti proportion was lower than its optimal amount, with the increase of Bi–Ti proportion, it could increase the Bi–O polyhedral, which acted as electron trapping centers to prolong the life of carriers, and increase active sites and number of substrates adsorbed due to the smaller crystal size, thereby improving the photocatalytic activities; however, when the Bi–Ti proportion was higher than its optimum amount, higher concentration of Bi often gave rise to particle agglomeration of Bi_2O_3 with severe nanocrystal heterojunction decline, which could cause a decrease in the photocatalytic activities. To evaluate the role of heterojunction on the photocatalytic activities, we used a direct mixing method to prepare Bi–Ti–0.0175–420 composite powder as comparison with the nonaqueous sol–gel technique. The as-prepared Bi–Ti–0.0175–420 composite powder showed a rather lower photocatalytic performance, where the degradation ratio was just 5% in 5 h. This suggested it was desirable to prepare heterojunction composite with intimate contact between heterophase nanoparticles of Bi_2O_3 and TiO_2 to make interparticle electron transfer more efficient and achieve a higher photocatalytic performance.

We also noticed that the photocatalytic activity decreased steadily with increasing calcination temperatures (Fig. 5b). Calcination at higher temperatures, to promote better crystallinity, often gave rise to particle agglomeration and reduced bulk defects and surface areas, and thus lowered the activity of the catalyst [28]. However, when the calcination temperature decreased to 320 °C, there was no or negligible photocatalytic activity for the obtained black powders because the residual carbon from organic precursors was not completely removed during the thermal treatment.

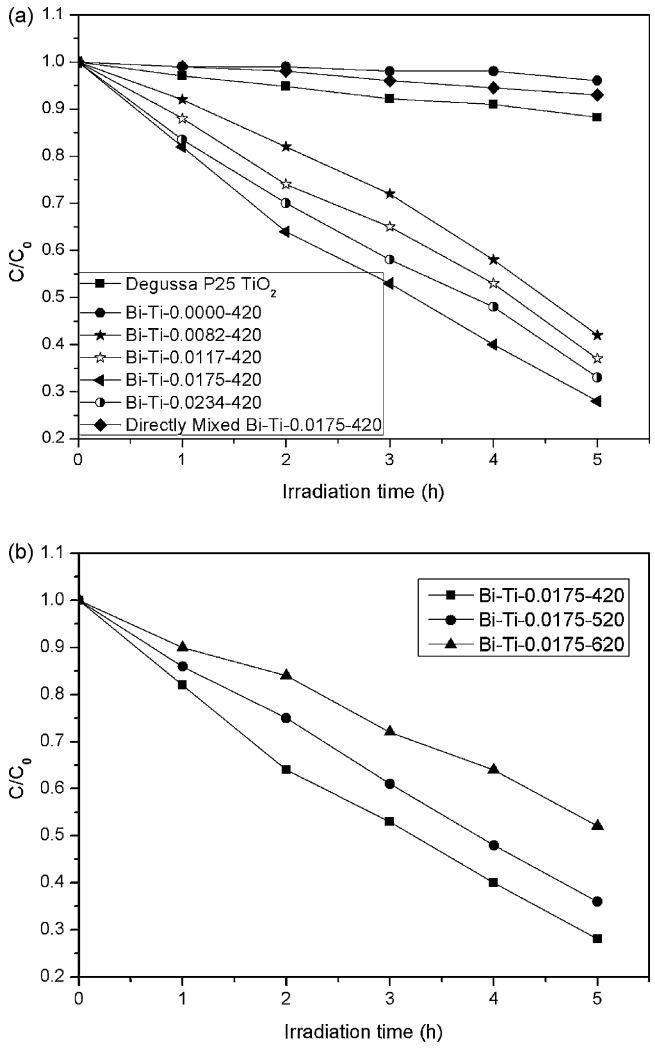

Fig. 5. (a) Effect of Bi–Ti proposition on the photocatalytic activities of Bi–Ti–*x*–420 and (b) effect of calcination temperature on the photocatalytic activities of Bi–Ti–0.0175.

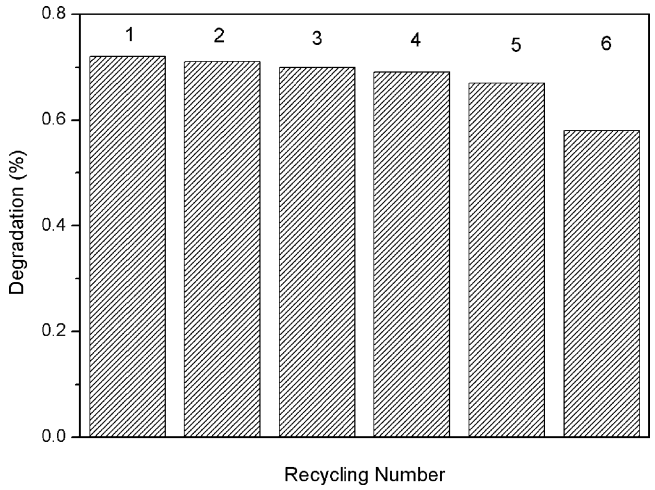

Fig. 6. Cycling runs in the photocatalytic degradation of MO in the presence of Bi–Ti–0.0175–420 under visible light.

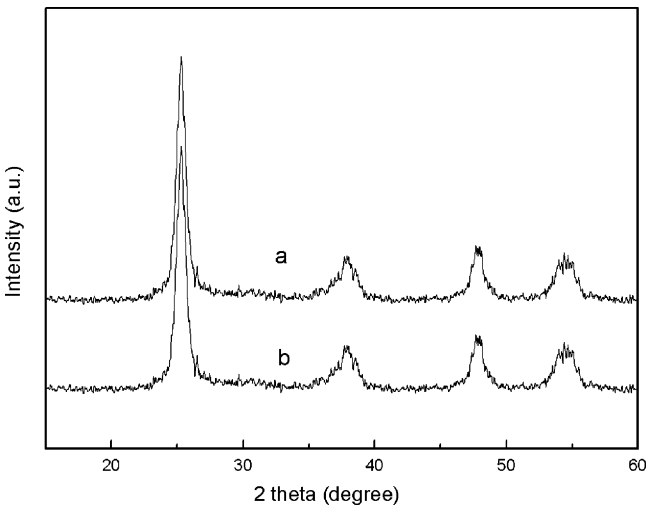

Fig. 7. XRD patterns of Bi–Ti–0.0175–420 (a) before photodegradation and (b) after photodegradation.

3.6. Photocatalytic stability in degradation reaction

To test the stability of the photocatalysts, Bi–Ti–0.0175–420 as a representative photocatalyst, was used for five recycles of photodegradation of MO. As indicated in Fig. 6, the catalytic activities exhibited no significant decrease and kept photostable. The decrease of the catalytic activity after five recycles may partly resulted from incomplete separation of the catalyst powders from liquid and the catalyst loss during the process of washing. Furthermore, characterizations had been performed to test the stability of Bi–Ti–0.0175–420. The detailed X-ray photoelectron survey spectra for Ti 2p and Bi 4f were shown in Fig. 1. There was only a small decrease of intensity before and after the catalytic reactions, which indicated that the oxidation state of Ti and Bi remained stable in the reaction process. The XRD patterns in Fig. 7 gave nearly the same, therefore, the crystal phase of Bi–Ti–0.0175–420 did not change obviously and possessed stability in the photocatalytic process.

4. Conclusions

The nonaqueous sol–gel method and CTAB as a dispersant were used to prepare a series of Bi_2O_3–TiO_2 composites, which exhibited better photocatalytic activities and stability in degradation of MO under visible light irradiation. The Bi_2O_3–TiO_2 photocatalyst with Bi–Ti proportion of 0.0175 showed the best performance in the experimental conditions. The calcination temperature also strongly influenced the activity of the samples: the photocatalytic degradation of MO decreased gradually with increasing calcination temperature from 420 to 620 °C. Furthermore, the introduction of Bi_2O_3 could effectively suppress phase transformation of anatase-to-rutile, prevent the over growth of crystallites and enhance visible light absorption in comparison with pure TiO_2.

Acknowledgements

We gratefully acknowledge financial support by the National Natural Science Foundation of China (NSFC) 20876109 and 20776016 as well as Program for New Century Excellent Talents in University of China MOE.

References

[1] Y.Y. Lv, L.S. Yu, H.Y. Huang, H.L. Liu, Y.Y. Feng, J. Alloys Compd. 488 (2009) 314–319.

[2] C.G. Silva, W.D. Wang, J.L. Faria, J. Photochem. Photobiol. A: Chem. 181 (2006) 314–324.
[3] P.A. Pekakis, N.P. Xekoukoulotakis, D. Mantzavinos, Water Res. 40 (2006) 1276–1286.
[4] J.H. Jho, D.H. Kim, S.J. Kim, K.S. Lee, J. Alloys Compd. 459 (2008) 386–389.
[5] G. Li, F. Liu, Z. Zhang, J. Alloys Compd. 493 (2010) L1–L7.
[6] M.R. Hoffmann, S.T. Martin, W. Choi, D.W. Bahnemann, Chem. Rev. 95 (1995) 69–96.
[7] Y. Bessekhouad, D. Robert, J.V. Weber, J. Photochem. Photobiol. A: Chem. 163 (2004) 569–580.
[8] Y. Bessekhouad, D. Robert, J.V. Weber, Catal. Today 101 (2005) 315–321.
[9] H.J. Huang, D.Z. Li, X.Z. Fu, Environ. Sci. Technol. 43 (2009) 4164–4168.
[10] S.Y. Chai, Y.J. Lim, M.H. Jung, A.K. Chakraborty, W.I. Lee, J. Catal. 262 (2009) 144–149.
[11] M. Shang, W.Z. Wang, L. Zhang, S.M. Sun, L. Wang, L. Zhou, J. Phys. Chem. C 113 (2009) 14727–14731.
[12] K.Y. Song, M.K. Park, Y.T. Kwon, H.W. Lee, W.I. Chung, I. Lee, Chem. Mater. 13 (2001) 2349–2355.
[13] S.J. Parzi, A.R. Mahjoub, J. Alloys Compd. 486 (2009) 805–808.
[14] Y.J. Kim, B. Gao, S.Y. Han, M.H. Jung, C. Lee, W.I. Lee, J. Phys. Chem. C 113 (2009) 19179–19184.
[15] T.P. Ang, C.S. Toh, Y.F. Han, J. Phys. Chem. C 113 (2009) 10560–10567.
[16] Z.F. Bian, J. Zhu, S.H. Wang, H.X. Li, J. Phys. Chem. C 112 (2008) 6258–6262.
[17] L.Q. Jing, J. Wang, Y.C. Qu, Y.B. Luan, Appl. Surf. Sci. 256 (2009) 657–663.
[18] A. Hameed, V. Gombac, T. Montini, L. Felisri, P. Fornasiero, Chem. Phys. Lett. 483 (2009) 254–261.
[19] J.J. Xu, Y.H. Ao, D.G. Fu, C.W. Yuan, Appl. Surf. Sci. 255 (2008) 2365–2369.
[20] L.D. Vaisman, H.D. Wagner, G. Marom, Adv. Colloid Interf. Sci. 128 (2006) 37–46.
[21] H. Yan, X.H. Zhang, J.M. Wu, L.Q. Wei, X.G. Liu, B.S. Xu, Powder Technol. 188 (2008) 128–132.
[22] M.J. Assael, I.N. Metaxa, J. Arvanitidis, D. Christofilos, C. Lioutas, Int. J. Thermophys. 26 (2005) 647–664.
[23] X.H. Wu, W. Qin, W.D. He, J. Mol. Catal. A: Chem. 261 (2007) 167–171.
[24] X.S. Peng, G.W. Meng, J. Zhang, L.X. Zhao, J. Phys. D: Appl. Phys. 34 (2001) 3224–3228.
[25] X.H. Xu, M. Wang, Y. Hou, W.F. Yao, J. Mater. Sci. Lett. 21 (2002) 1655–1656.
[26] S. Rengaraj, X.Z. Li, P.A. Tanner, Z.F. Pan, G.K.H. Pang, J. Mol. Catal. A: Chem. 247 (2006) 36–43.
[27] X.H. Xu, M. Wang, Y. Hou, W.F. Yao, D. Wang, H. Wang, J. Master Sci. Lett. 21 (2002) 1655–1656.
[28] C. Xie, Z.L. Xu, Q.J. Yang, B.Y. Xue, Y.D. Du, Mater. Sci. Eng. B 112 (2004) 34–41.